EBioMedicine 5 (2016) 93–104

Contents lists available at ScienceDirect

EBioMedicine

journal homepage: www.ebiomedicine.com

Research Paper

miR-378 Activates the Pyruvate-PEP Futile Cycle and Enhances Lipolysis to Ameliorate Obesity in Mice

Yong Zhang [a,1], Changyin Li [a,1], Hu Li [a], Yipeng Song [b], Yixia Zhao [a], Lili Zhai [a], Haixia Wang [c], Ran Zhong [a], Huiru Tang [b], Dahai Zhu [a,*]

[a] The State Key Laboratory of Medical Molecular Biology, Institute of Basic Medical Sciences, Chinese Academy of Medical Sciences and School of Basic Medicine, Peking Union Medical College, Beijing 100005, PR China

[b] Key Laboratory of Magnetic Resonance in Biological Systems, State Key Laboratory of Magnetic Resonance and Atomic and Molecular Physics, Centre for Biospectroscopy and Metabonomics, Wuhan Institute of Physics and Mathematics, Chinese Academy of Sciences, Wuhan 430071, PR China

[c] Gladstone Institute of Cardiovascular Disease and Roddenberry Center for Stem Cell Biology and Medicine at Gladstone, San Francisco, CA 94158, USA

ARTICLE INFO

Article history:
Received 13 November 2015
Received in revised form 25 January 2016
Accepted 28 January 2016
Available online 11 March 2016

Keywords:
miR-378
Futile cycle
Lipolysis
Energy homeostasis
Obesity
SCD1

ABSTRACT

Obesity has been linked to many health problems, such as diabetes. However, there is no drug that effectively treats obesity. Here, we reveal that miR-378 transgenic mice display reduced fat mass, enhanced lipolysis, and increased energy expenditure. Notably, administering AgomiR-378 prevents and ameliorates obesity in mice. We also found that the energy deficiency seen in miR-378 transgenic mice was due to impaired glucose metabolism. This impairment was caused by an activated pyruvate-PEP futile cycle via the miR-378-Akt1-FoxO1-PEPCK pathway in skeletal muscle and enhanced lipolysis in adipose tissues mediated by miR-378-SCD1. Our findings demonstrate that activating the pyruvate-PEP futile cycle in skeletal muscle is the primary cause of elevated lipolysis in adipose tissues of miR-378 transgenic mice, and it helps orchestrate the crosstalk between muscle and fat to control energy homeostasis in mice. Thus, miR-378 may serve as a promising agent for preventing and treating obesity in humans.

1. Introduction

Obesity is a major cause of debilitating diseases such as type 2 diabetes, hypertension, and cardiovascular disease (Olshansky et al., 2005), which have a devastating impact on our quality of life and lifespan (Olshansky et al., 2005). Yet, our search for drugs that prevent and treat obesity has become one of the most challenging areas in drug discovery.

Glucose and lipids are macromolecules that the body uses as fuel to regulate energy fluxes and meet metabolic demands. This fuel is largely stored in skeletal muscle and adipose tissues, whose metabolic communication determines how the fuel will be selected and used under physiological and pathological conditions (Li et al., 2015; Lu et al., 2014; Shimizu et al., 2015; Viscarra and Ortiz, 2013). When this communication is dysregulated, metabolic disorders, including obesity, diabetes, and metabolic syndrome, often develop (Bilski et al., 2015; Bleau et al., 2014). While much work has focused on either glucose metabolism in muscle or lipid metabolism in adipose tissues, we do not know how communication between these processes maintains metabolic homeostasis in the body.

Metabolism is regulated by microRNAs. For example, miR-378 and miR-378*, which are embedded within the first intron of the peroxisome proliferator-activated receptor γ coactivator 1β (*Ppargc1b* or *Pgc-1β*) gene, are preferentially expressed in metabolically active tissues, skeletal muscle, and brown adipose tissue (BAT) (Carrer et al., 2012; Eichner et al., 2010). They also critically regulate fatty acid metabolism in mitochondria by targeting carnitine O-acetyltransferase (*Crat*) and Mediator 13 (*MED13*) in liver (Carrer et al., 2012). Hepatic miR-378 controls liver glucose and lipid homeostasis by modulating insulin signaling (Liu et al., 2014), and miR-378 stimulates brown-fat expansion by targeting phosphodiesterase 1b (*Pde1b*) (Pan et al., 2014). Furthermore, miR-378* induces a glycolytic shift by targeting the PGC-1β partners, *ERR*γ and *GABPA*, in breast cancer cells (Eichner et al., 2010), and levels of miR-378 expression is inversely correlated with the loss of adipose tissue in cancer cachexia in humans (Kulyte et al., 2014).

Here, we report that miR-378 prevents and treats obesity in mice by activating the pyruvate-phosphoenolpyruvate (pyruvate-PEP) futile cycle in the muscle and enhancing lipolysis in adipose tissues. Notably, we also show that transgenic mice globally overexpressing miR-378 provide a genetic system for investigating the metabolic crosstalk between different tissues at whole-body levels. Our significant findings support an unprecedented role of the pyruvate-PEP futile cycle in stimulating lipolysis in adipose tissues to regulate whole-body energy homeostasis.

* Corresponding author.
E-mail address: dhzhu@pumc.edu.cn (D. Zhu).
[1] Co-first authors.

http://dx.doi.org/10.1016/j.ebiom.2016.01.035

2. Materials and Methods

2.1. Mice and Animal Care

All animal procedures were approved by the Animal Ethics Committee of Peking Union Medical College, Beijing (China). Mice were housed in the animal facility and given free access to water and a standard diet (SD) of rodent chow or a high-fat diet (HFD) according to the experimental design. miR-378 transgenic (Tg) mice were generated by the Model Animal Research Center of Nanjing University. Two transgenic lines were established from two founders identically created with the same plasmid DNA construct containing miR-378 precursor sequences and the beta-actin promoter for driving the transgene miR-378 expression (Figure S1A), and the gender- and age-matched wild-type littermates were served as control group throughout all experiments presented in the study. C57BL/6 male mice (Vital River Laboratories Company in Beijing) were used in the experiments treated with AgomiR-378.

2.2. Metabolic-Chamber Analysis

Metabolic phenotyping of wild-type (Wt, n = 8) and miR-378 Tg (n = 8) mice on a standard diet was performed using Columbus × Oxymax/CLAMS metabolic-chamber analysis at the animal center at Peking Union Medical College.

2.3. Glucose and Insulin Tolerance Tests

Overnight-fasted mice were given intraperitoneal (i.p.) injections of glucose (2 mg/g body weight) for the glucose-tolerance test (GTT). For insulin-tolerance tests (ITT), mice fasted for 4 h and then were given 0.5 mU insulin/g body weight by i.p. injection (Novolin). Blood glucose was determined with a Lifescan One Touch glucometer.

2.4. Prevention and Treatment of HFD-induced Obesity with AgomiR-378

Cholesterol-modified AgomiR-378 and control oligos were ordered from RiboBio (Guangzhou, China). For the prevention study, C57BL/6 mice were fed an HFD, or an SD as control. During HFD feeding, AgomiR-378 was consecutively administered to the mice weekly by tail–vein injection (20 μg/g body weight) for 8 weeks. AgomiR-378 and control oligos were administered to 10 male mice, respectively. For treatment experiments, C57BL/6 mice were fed an HFD for 11 weeks to induce obesity, with mice fed an SD as control. Then, obese mice were treated weekly with AgomiR-378, or scrambled oligo as control, by tail–vein injection (20 μg/g body weight) for 4 consecutive weeks. After the last injection, mice underwent GTT and ITT and were then sacrificed for sampling.

2.5. Adenovirus-Mediated Akt1 Rescue Experiments

Constitutively active Akt1, with myristylation-signal sequences (GSSKSKPKSR) in its N-terminus and a Myc-tag at its C-terminus, was subcloned from pUSE-myr-Akt1. The recombinant adenoviruses were packaged by Hanheng Biotechnology Corporation (Shanghai, China). Viruses were administered to miR-378 Tg and Wt mice through tail-vein injections with 1×10^9 PFU in 0.25 ml PBS. Viruses packaged with empty vector served as negative control. Injection of the viruses did not affect food intake in control or treated animals. Mice were sacrificed 10 days after the adenovirus injection and sampling.

2.6. C2C12-Cell Culture and Transfection

C2C12-cell culture was conducted as previously described (Wu et al., 2015a, 2015b). Briefly, C2C12 cells were cultured in growth medium consisting of Dulbecco's modified Eagle's medium (DMEM; Gibco) supplemented with 10% fetal bovine serum (FBS) at 37 °C in a 5% CO_2 atmosphere. At 50–60% confluence, cells were switched to differentiation medium (DMEM supplemented with 2% horse serum). C2C12 cells were transfected with miR-378 mimic and control oligos using Lipofectamine 2000. Twenty-four h after transfection, cells were lysed and evaluated for levels of Akt1 protein by Western blotting.

2.7. Adipogenesis In Vitro and Transfection

3T3-L1 cells were obtained from ATCC. Maintenance and adipogenesis of 3T3-L1 cells were as described previously using methylisobutylxanthine, dexamethasone, and insulin (MDI) (Hemati et al., 1997). To induce adipogenesis, cells that were confluent for 2 days (day 0) were treated with 10% FBS, 1 μM dexamethasone, 0.5 mM methylisobutylxanthine, 1 μg/ml insulin, and 5 μM troglitazone. On day 2, cells were fed DMEM containing 1 μg/ml insulin and 10% FBS. On day 4, cells were refed with DMEM containing 10% FBS and were transfected with AgomiR-378 or *Scd1*-overexpression plasmid using Lipofectamine 2000. Lipid accumulation in adipocytes was visualized by staining with Oil Red-O.

2.8. Western-Blot Analysis

Mouse tissues or cells were lysed in lysis buffer containing 50 mM Tris pH 7.5, 150 mM NaCl, 0.5% Nonidet P40, and protease and phosphatase inhibitors. Protein lysates were resolved by SDS-PAGE, transferred to a polyvinylidene fluoride (PVDF) membrane, and immunoblotted with primary antibodies against total Akt1 (Cell Signaling 2938, 1:1000), phosphorylated Akt1 (Santa Cruz sc7985, 1:2000), total FoxO1 (Cell Signaling 2880, 1:300), phosphorylated FoxO1 (Cell Signaling 9464s, 1:300), Myc-tag (Millipore 05–724, 1:2000), GAPDH (Millipore, 1:10,000), or β-actin (Sigma, 1:20,000). Membranes were washed in TBS washing buffer for 30 min, incubated with horseradish peroxidase (HRP)–conjugated secondary antibodies (Zhongshanjinqiao Corporation, 1:2000) for 1 h at room temperature, and washed in TBS washing buffer for 30 min. Each membrane was then placed into Detection Solution (Thermo), incubated for 1 min at room temperature, and exposed to X-ray film.

2.9. Real-Time Quantitative PCR (RT-qPCR) Analysis

Total RNA from mouse tissues or cells was extracted with Trizol reagent (Invitrogen). Expression of miR-378 was determined with the miR-378-specific TaqMan probe (Applied Biosystems) and the iQ5 multicolor Real-Time PCR Detection System (Bio-Rad). U6 snRNA was used for normalization. mRNA expression was analyzed with SsoFast EvaGreen qPCR Master Mix (Bio-Rad) and normalized to GAPDH. All primers used for RT-qPCR are listed in Table S1.

2.10. Target-Gene Prediction and Luciferase-Reporter Assays

miR-378 targets were predicted with TargetScan. The wild-type and mutant forms of 3′-UTRs in mouse *Akt1* and *Scd1* were amplified by PCR and cloned into the pGL3-Control vector. HEK-293 cells were co-transfected with *Akt1*–3′-UTR or *Scd1*–3′-UTR and miR-378 mimics. Empty pGL-3 vector was a negative control. A Renilla-luciferase plasmid was co-transfected with a firefly-luciferase construct as a transfection control. The results are expressed as firefly-luciferase activity relative to Renilla-luciferase activity.

2.11. Measurement of DNA Content

DNA content was measured and used to evaluate adipocyte numbers in a given fat depot. To measure genomic DNA content, fat depots were excised, weighted, and minced. Fat samples with equal amounts were digested with 10 mM Tris buffer (pH 7.5) containing protease K

(0.4 mg/ml), and genomic DNA was precipitated with ethanol. DNA content was calculated as per fat depot.

2.12. Oil Red-O Staining

Cells were fixed with 3.7% (*W*/*V*) formaldehyde for 15 min at room temperature and then stained with 0.3% (*W*/*V*) Oil Red-O solution in 60% isopropyl alcohol for 1 h. Excess staining was removed by briefly washing with water.

2.13. Histology

Adipose-tissue samples were fixed in 10% buffered formalin and embedded in paraffin for Hematoxylin and Eosin (H&E) staining. Cell or nuclei numbers per view were quantified by analyzing randomly selected fields from adipose-tissue sections using the Image Pro Plus 5.1 software (Olympus). Skeletal muscle samples were immediately frozen with liquid nitrogen-cooled isopentane after dissection and sectioned on a cryostat microtome. α-GPDH and SDH staining was performed as described (Dunn and Michel, 1997).

2.14. Enzymatic-Activity Assay in Skeletal Muscle

Enzymatic activities of pyruvate dehydrogenase (PDH) were measured with a pyruvate dehydrogenase kit (Abcam, ab110671) per manufacturer's instructions. 6-phosphofructokinase (PFK) activities were examined with a 6-phosphofructokinase kit (Cominbio, NY3) per manufacturer's instructions. Enzymatic activities of phosphoenolpyruvate carboxykinase (PEPCK) were measured with a PEPCK activity kit (Nanjing Jian Cheng) per manufacturer's instructions.

2.15. Muscle-Homogenates Analysis

Levels of several metabolites in muscle homogenates were measured with kits assaying pyruvate (Cominbio, NY5), lactate (Nanjing Jian Cheng, A019-2), acetyl CoA (Cominbio, MY7-1), and the ADP/ATP-ratio (Sigma, MAK135).

2.16. Serum-Sample Analysis

Measurements of insulin, free-fatty acids (FFA; Senbeijia Corporation, China), and lactate level in serum (Nanjing Jian Cheng, A019-2) were performed with kits per manufacturer's instructions. Insulin levels in plasma were measured by ELISA (Chrystal Chem).

2.17. Fatty-Acid Analysis

Fatty acids were methylated following the protocol previously described (Xu et al., 2010) with few modifications. Briefly, 10 mg of adipose tissue was homogenized in 500 μL methanol by a tissue-lyser (QIAGEN TissueLyser II, Germany) at 20 Hz for 90 s. Then, 100 μL tissue homogenate and 20 μL internal standards (methyl heptadecanoate, methyl tricosanate, and BHT) were mixed with 1 mL of a methanol–hexane mixture (4:1, *v*/v) in a Pyrex tube. The Pyrex tube was cooled over liquid nitrogen and then added to 100 μL pre-cooled acetyl chloride. After incubation in the dark at 25 °C for 24 h, samples were neutralized with K_2CO_3 solution and extracted by mixing with 200 μL hexane 4 times. After evaporation of the resulted supernatant, the extracted power was redissolved in 100 μL hexane before GC-FID analysis.

Methylated fatty acids were determined on a Shimadzu GC-2010 Plus GC–MS spectrometer (Shimadzu Corporation, Japan) equipped with a flame-ionization detector (FID), a mass spectrometer, and a DB-225 capillary–GC column (Agilent technology, USA). Then, 1 μL of redissolved solution was added through the injection port with a splitter (1:60). The temperature in the injection port and FID is 230 °C. Fatty acids were identified and quantified with the standards. The unit of micromole fatty acids per liter of plasma is represented as the mean ± standard deviation. Except for directly detected results, saturated fatty acids (SFAs), unsaturated fatty acids (UFAs), monounsaturated fatty acids (MUFAs), and polyunsaturated fatty acids (PUFAs) were also calculated. In addition, we also calculated ratios that reflect the activities of desaturases, including D5D (C20:4n6/C20:3n6), D6D (C18:3n6/C18:2n6), SCD16 (C16:1n7/C16:0), and SCD18 (C18:1n9/C18:0).

2.18. Statistical Analysis

Values are presented as means ± s.e.m. The statistical significance of the difference between two means was calculated with a Student's *t*-test (two-tailed distribution, two-sample unequal variance) and displayed as $p < 0.05$ (one asterisk), $p < 0.01$ (two asterisks), or $p < 0.001$ (three asterisks). The tests were performed using Microsoft Excel, in which the test type is always set to two-sample equal variance.

3. Results

3.1. miR-378 Transgenic Mice Have Increased Catabolism and Reduced Fat Mass

To investigate how miR-378 controls whole-body energy homeostasis *in vivo*, we generated two lines (C and D lines) of transgenic mice (Tg) in which the miR-378 transgene was globally overexpressed under the control of the *β-actin* promoter (pCAGGS) (Figs. 1A, B, S1A, and S1B). miR-378 Tg mice had significantly reduced body weight compared to gender- and age-matched wild type littermates (Figs. 1C, S1C, S1D, and S1E). They showed the greatest reduction in organ mass in the muscle, inguinal white adipose tissue (iWAT), and gonadal white adipose tissue (gWAT) (Fig. 1D, E, and F), but no change in the mass of other organs (Fig. S1F). Interestingly, we did not observe a change in the number of adipocytes (Fig. 1G) or the expression of adipogenesis marker genes (Fig. 1H), indicating that adipogenesis was not affected in miR-378 mice. However, these mice had smaller adipocytes in both BAT and WAT, indicating increased lipid catabolism in fat tissues (Fig. 1I and J). They also displayed increased expression of lipid metabolism genes (Fig. 1K). These findings suggest that the reduced fat mass in miR-378 Tg mice is mainly due to reduced adipocyte size caused by significantly increased lipid catabolism rather than reduced numbers of adipocytes in adipose tissues. Because our two lines of miR-378 Tg mice have a similar phenotype, we further characterized only one of our lines in detail.

3.2. miR-378 Tg Mice Display Increased Energy Expenditure

To further validate the enhanced catabolism in adipose tissues of miR-378 Tg mice, we measured energy influx and consumption in the whole bodies of both miR-378 Tg and wild-type (Wt) mice with metabolic-chamber analysis. miR-378 Tg mice had a significant overall increase in body O_2 consumption (Figs. 2A and S2A), CO_2 production (Figs. 2B and S2B), and energy expenditure (Figs. 2C **and S2C**). These results were correlated with significantly increased expression of *Ucp1* in BAT of miR-378 Tg mice (Fig. 2D). Interestingly, these mice consumed remarkably more food and water than controls (Fig. S2D and S2E). These data show that miR-378 Tg mice increased their energy expenditure under normal physiological conditions.

Next, we determined the metabolic mechanism underlying the increased energy expenditure in miR-378 Tg mice. First, we found that expression of lipolytic genes was increased in miR-378 Tg mice (Fig. 2E), supporting enhanced lipolysis in WAT. We also found increased expression of genes related to lipid catabolism in both BAT and skeletal muscle of miR-378 Tg mice (Figs. 2F and S2F). As consequence of the increased energy expenditure, we observed decreased levels of free fatty acids (FFA) in serum of miR-378 Tg mice compared to their Wt littermates (Fig. 2G).

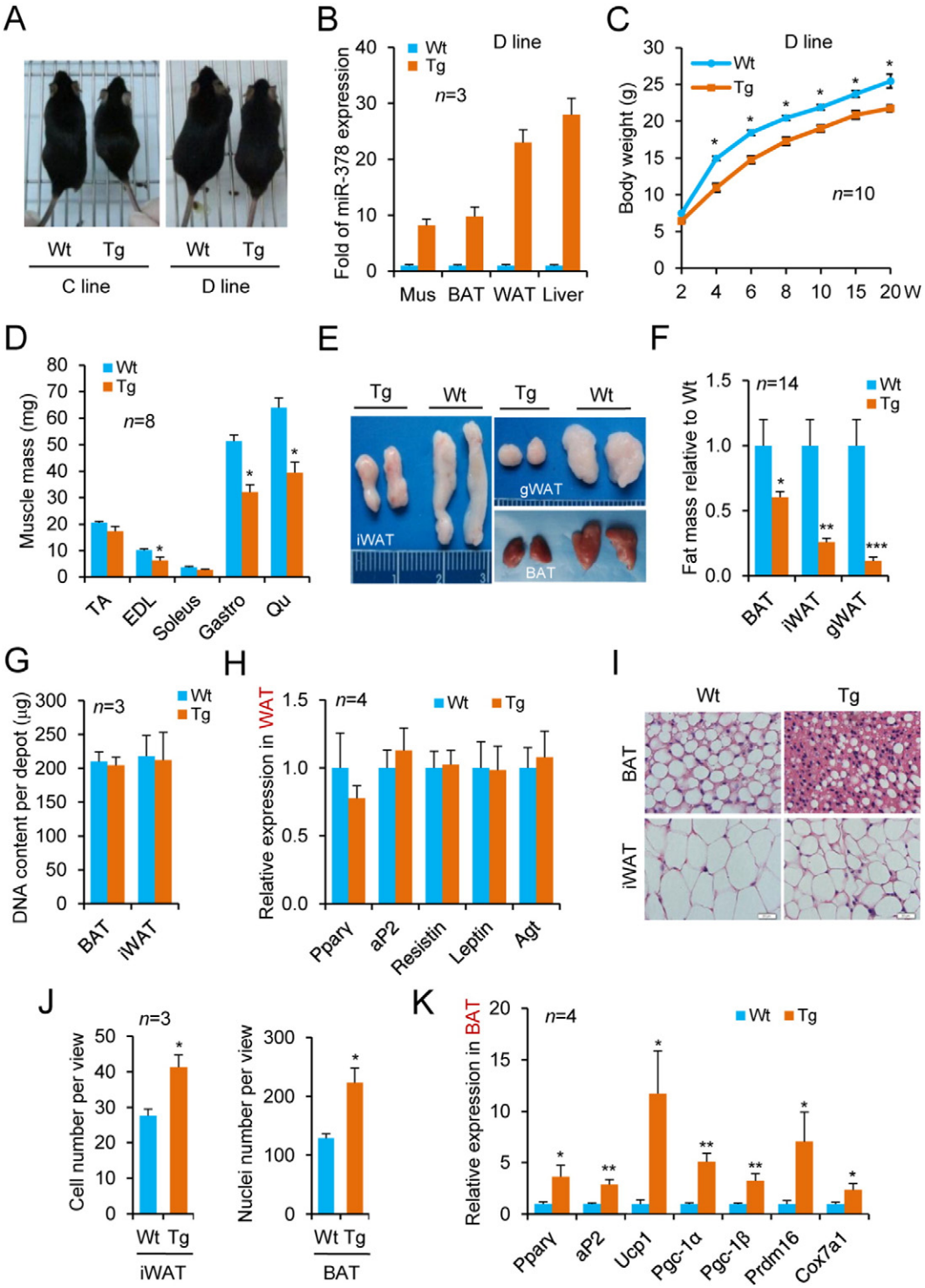

Fig. 1. miR-378 transgenic mice have reduced fat mass and increased catabolism. (A) Representative images of two lines of 6-week-old wild-type (Wt) and miR-378-transgenic (Tg) female mice fed normal chow. (B) miR-378 overexpression in skeletal muscle (Mus), brown-adipose tissue (BAT), white-adipose tissue (WAT), and liver of Tg mice. (C) Body weight of Tg and Wt (female) mice fed normal chow at the indicated ages (weeks, w). (D) Weight of muscle groups from 8-week-old Wt and Tg mice (female). *tibialis anterior* (TA), *gastrocnemius* (Gastro), *extensor digitorum longus* (EDL), *quadriceps* (Qu). (E) Fat pads from 12-week-old Tg and Wt littermates (female). Inguinal WAT (iWAT), gonadal WAT (gWAT), and BAT. (F) Relative fat weight of 12-week-old Tg and Wt mice. (G) Genomic DNA content per fat depot. n = 3 female mice at 12-weeks-old per group. (H) Relative mRNA levels of adipogenic markers in WAT by RT-qPCR. n = 4 female mice at 12-weeks-old. (I) Hematoxylin and eosin (H&E) staining of adipose tissue from 12-week-old female Wt and Tg mice. Scale bar, 20 μm. (J) Cell number per view (left) of iWAT section presented in (I), and nuclei number per view (right) on BAT section presented in (I). (K) Relative mRNA levels of adipogenic markers and metabolic regulators in BAT by RT-qPCR. n = 4 female mice at 12-week-old. Data are presented as means ± s.e.m. Statistical analysis was done using Student's unpaired *t*-test. $^{*}P < 0.05$, $^{**}P < 0.01$, $^{***}P < 0.001$. See also Fig. S1.

We then examined glucose metabolism in our miR-378 Tg mice. We found that these mice had slightly elevated levels of blood glucose when they were fed *ad libitum*, which significantly increased at a fasting state (Fig. 2H). Consistent with this finding, miR-378 Tg mice exhibited normal insulin sensitivity during insulin-tolerance tests (ITTs) (Fig. 2I), but impaired glucose metabolism in glucose-

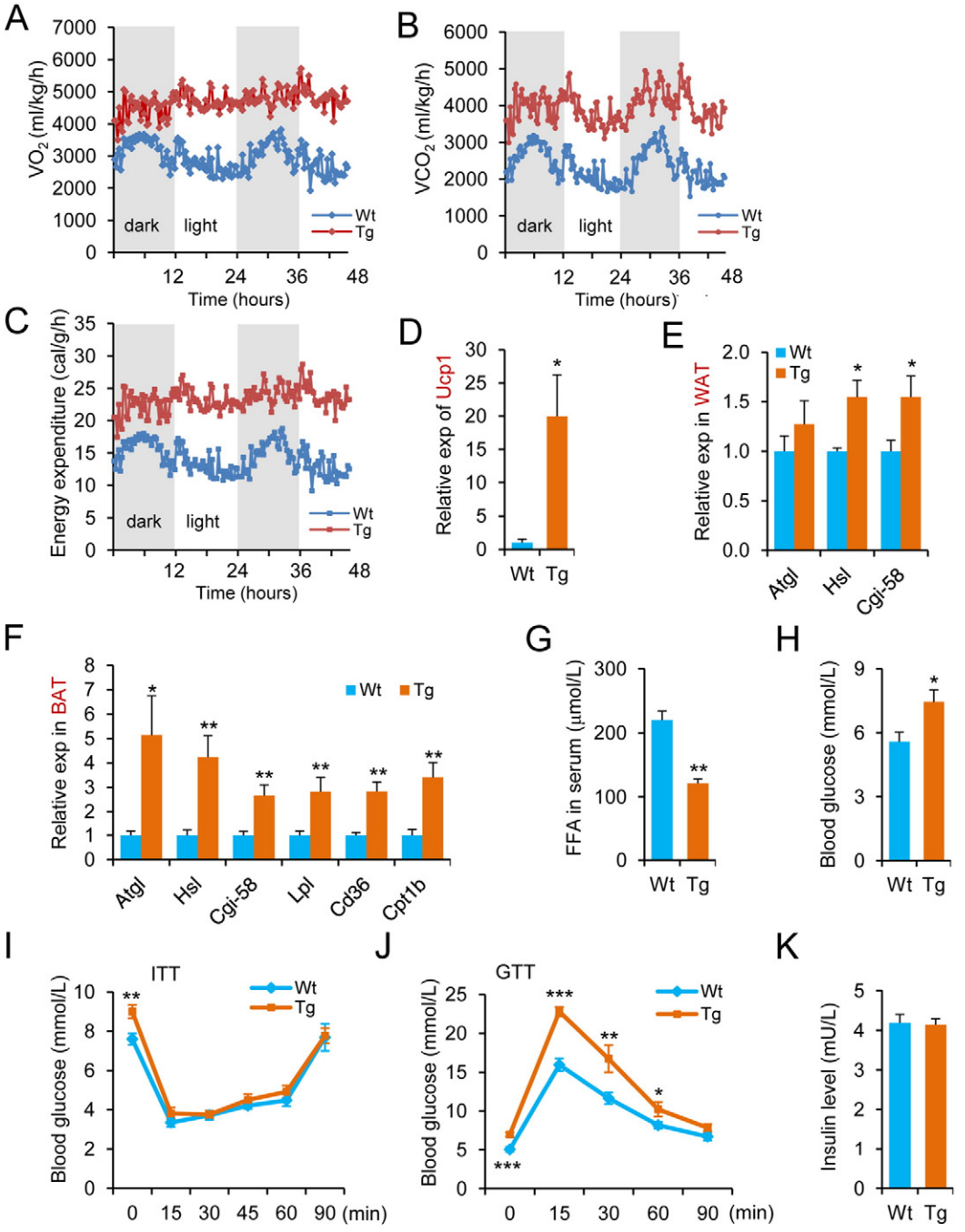

Fig. 2. miR-378 Tg mice display increased energy expenditure. (A–C) O_2 consumption (A), CO_2 production (B), and energy expenditure (C) by metabolic-chamber analysis of Tg and Wt mice. n = 8 12-week-old female mice for each group. (D) Relative expression (exp) of the *Ucp1* gene in BAT of Wt and Tg mice. n = 4 12-week-old female mice. (E) Relative expression of the lipolytic genes *Atgl*, *Hsl*, and *Cgi58* in WAT. n = 4 12-week-old female mice. (F) Relative expression of lipolytic (*Atgl*, *Hsl*, and *Cgi58*) and fatty-acid-utilization genes (*Lpl*, *Cd36*, *Cpt1b*) in BAT. n = 5 12-week-old female mice in each group. (G) Measurement of free-fatty acids (FFA) in serum. n = 5 12-week-old female mice in each group. (H) Blood glucose in Tg and Wt mice fasted for 16 h. n = 8 12-week-old female mice for each group. (I) Insulin tolerance test (ITT) of Wt (n = 6) and Tg (n = 5) mice at 12 weeks of age. (J) Glucose tolerance test (GTT) of 12-week-old Wt (n = 7) and Tg (n = 8) mice fasted for 16 h. (K) Insulin levels were measured on 12-week-old mice fasted for 16 h. n = 5 female mice in each group. Data are presented as means ± s.e.m. The statistical significance of the difference between two means was calculated using Student's unpaired *t*-test. $^{*}P < 0.05$, $^{**}P < 0.01$, $^{***}P < 0.001$. See also Fig. S2.

tolerance tests (GTTs) (Fig. 2J). Of note, the serum concentration of insulin was similar between miR-378 Tg and Wt mice (Fig. 2K). These implicate that the hyperglycemia we observed in miR-378 Tg mice was a result of dysregulated glucose homeostasis rather than decreased insulin secretion or insulin resistance in peripheral tissues. Furthermore, these data support that the energy deficiency we observed in miR-378 Tg mice is a result of elevated lipolysis and impaired glucose metabolism.

3.3. miR-378 Tg Mice Are Resistant to Obesity When Fed a High-Fat Diet

Next, we tested if miR-378 protects mice against obesity induced by a high-fat diet (HFD). We found that miR-378 Tg mice had a significantly lower body weight than Wt mice after 12-weeks on a HFD (Fig. 3A), even though both lines ate the same amount of food (Fig. 3B). Additionally, miR-378 mice has significantly less fat mass than Wt controls (Fig. 3C), which was supported by a reduced number of adipocytes

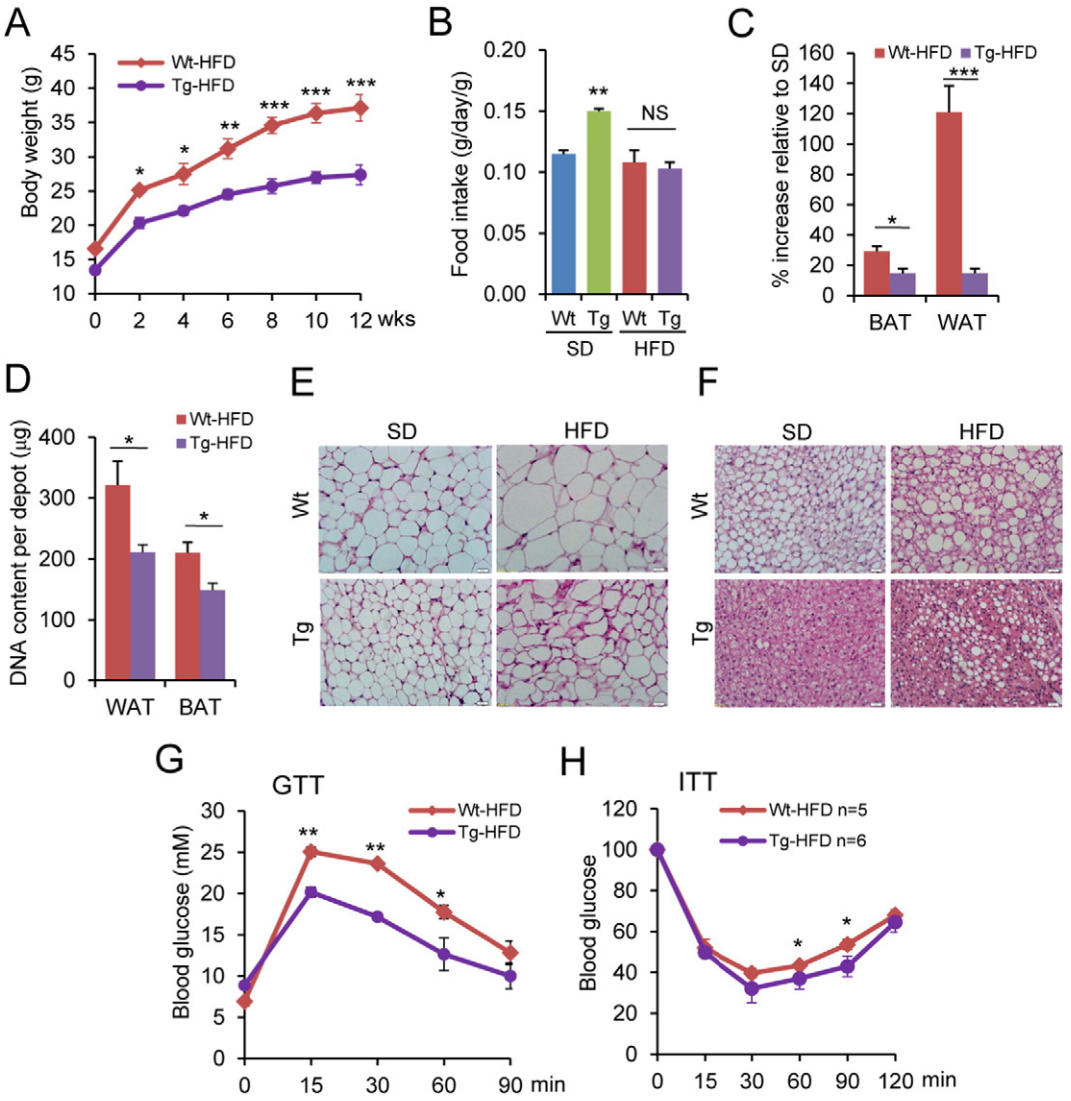

Fig. 3. miR-378 Tg mice are resistant to high-fat-diet-induced obesity. (A) Body weight of Wt (n = 7) and Tg (n = 6) mice on high-fat diet (HFD) for 12 weeks (wks). (B) Food intake measured in Wt and Tg mice fed an HFD and SD, respectively. n = 5 in each group. (C) Percentage of increased fat mass in Wt and Tg mice fed an HFD for 12 weeks relative to standard diet (SD) (n = 5 in each group). (D) Genomic DNA content per fat depot from Wt and Tg mice fed an HFD for 12 weeks. (E,F) Hematoxylin and eosin (H&E) staining for adipose tissue from Wt and Tg mice fed an HFD for 12 weeks. Scale bar, 20 μm. (G) Glucose-tolerance test (GTT) in 12-week HFD-fed Wt (n = 5) and Tg (n = 6) mice fasted for 16 h. Glucose levels were determined at baseline and at the indicated times after an i.p. glucose stimulus (1.5 mg/g body weight). (H) Insulin-tolerance test (ITT) in Wt (n = 5) and Tg (n = 6) mice fed an HFD for 12 weeks. Data are presented as means ± s.e.m. The statistical significance of the difference between two means was calculated with the Student's unpaired *t*-test. $^{*}P < 0.05$, $^{**}P < 0.01$, $^{***}P < 0.001$. NS, statistically non-significant.

(Fig. 3D) and their smaller size in both WAT (Fig. 3E) and BAT (Fig. 3F). Consistent with this finding, we observed significantly improved GTT and ITT in miR-378 Tg mice on an HFD (Fig. 3G and H).

3.4. Systemically Administering miR-378 Prevents and Ameliorates Obesity in Mice

We investigated whether systemically administering miR-378 (AgomiR-378) prevents HFD-induced obesity in C57BL/6 mice (Fig. S3A). We found that simultaneously injecting mice with AgomiR-378 while they were fed an HFD (Fig. S3B) significantly reduced their body weight (Fig. S3C) and weight gain (Fig. 4A), which was not due to reduced food intake (Fig. S3D) or lean mass (Fig. S3E). Interestingly, in AgomiR-378 mice fed an HFD, BAT mass was not reduced (Fig. 4B), but both iWAT and gWAT mass increased significantly less than control mice (Fig. 4B). These results were further supported by a smaller adipocyte size and decreased lipid deposits (Fig. 4C) in AgomiR-378 mice. These mice fed with HFD also showed improved GTT (Fig. 4D) and nearly normal ITT (Fig. 4E).

Next, we treated mice with diet-induced obesity (DIO) by systematically administrating AgomiR-378 for four weeks (Fig. S4A). At end of treatment, DIO mice treated with AgomiR-378 had reduced body weight and weight gain compared to control mice (Fig. S4B and Fig. 4F). Notably, in AgomiR-378-treated mice, we also found that WAT mass was remarkably decreased (31%), while BAT mass did not change compared with control mice (Fig. 4G). We also observed smaller adipocytes and less lipid deposits in both the BAT and WAT of DIO mice treated with AgomiR-378 (Fig. 4H). AgomiR-378 treatment did not alter food intake (Fig. S4C) or lean mass (Fig. S4D) in DIO mice; however, they displayed improved GTT (Fig. 4I) and ITT (Fig. 4J) compared with their control counterparts.

3.5. The Pyruvate-PEP Futile Cycle in Skeletal Muscle Causes Energy Deficiency in miR-378 Tg Mice

We speculated that the impaired glucose metabolism in miR-378 Tg mice might be the primary cause of their energy deficiency. Interestingly, we found that miR-378 Tg mice displayed increased expression of key

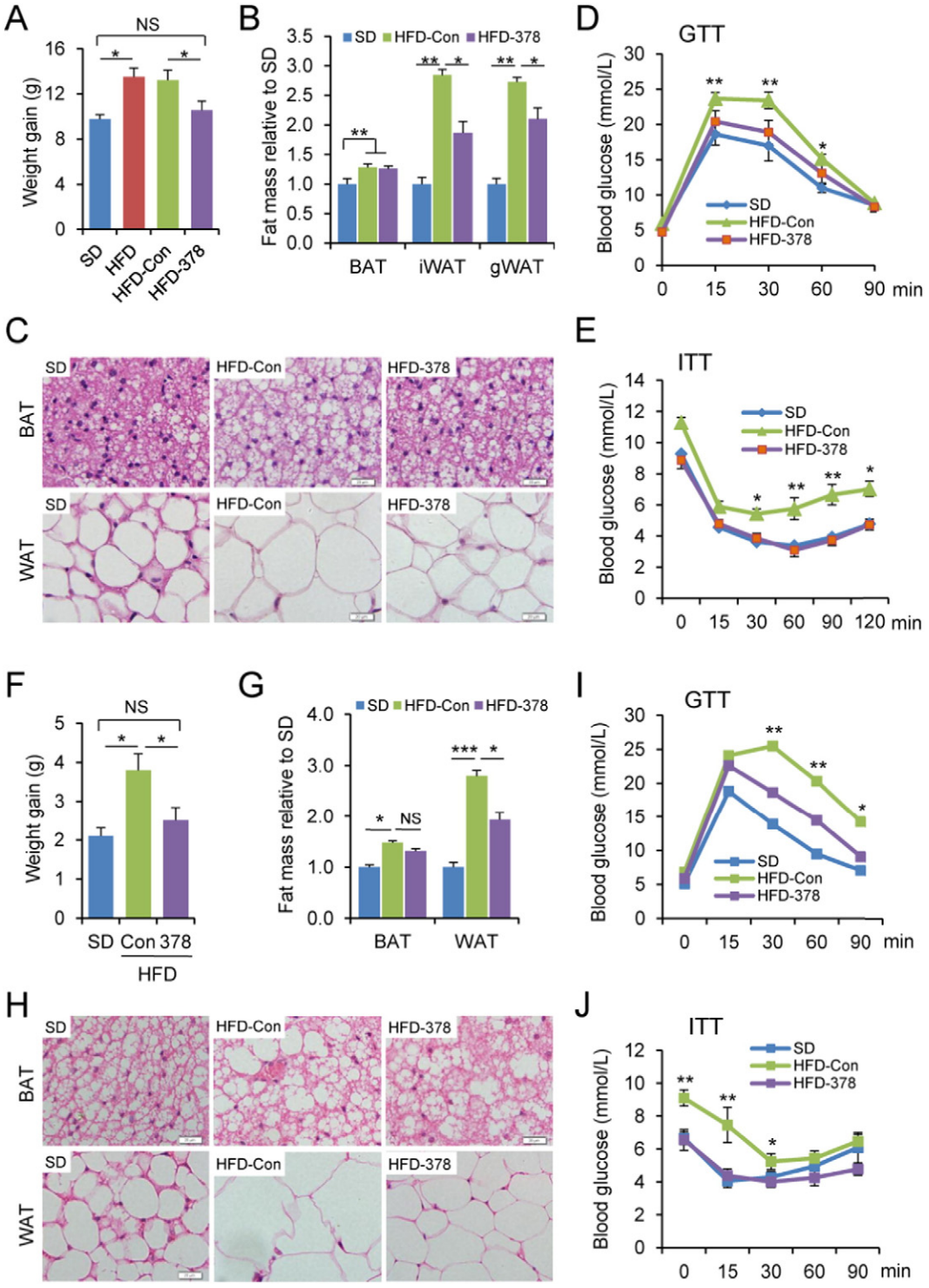

Fig. 4. Systematic administration of miR-378 prevents and ameliorates obesity in mice. (A–E) C57BL/6 mice fed a high-fat diet (HFD) or standard diet (SD) as control for 10 weeks. During HFD feeding, cholesterol modified AgomiR-378 (HFD-378) was administered (20 μg/g body weight) weekly for 8 consecutive weeks, which significantly prevented HFD-induced obesity (DIO) compared to control oligos (HFD-Con). n = 10 male mice in each group. (A) Reduced body-weight gain. (B) Reduced white-fat mass. (C) Reduced size of adipocytes and lipid droplets by Hematoxylin and Eosin staining (H&E). Scale bar, 20 μm. (D) Improved glucose-tolerance test (GTT). (E) Corrected insulin-tolerance test (ITT). (F–J) C57BL/6 mice were fed an HFD for 11 weeks to induce obesity (DIO). DIO mice were treated weekly with AgomiR-378 (HFD-378) or control oligos (HFD-Con) for 4 consecutive weeks. AgomiR-378 treatment (20 μg/g body weight) significantly ameliorates HFD-induced obesity compared to controls (HFD-Con). n = 10 male mice in each group. (F) Reduced body-weight gain. (G) Reduced white-fat mass. (H) Reduced size of adipocytes and lipid droplets from Hematoxylin and Eosin (H&E) staining. Scale bar, 20 μm. (I) Improved GTT. (J) Corrected ITT. Data are presented as means ± s.e.m. The statistical significance of the difference between two means was calculated using Student's unpaired *t*-test. $^{*}P < 0.05$, $^{**}P < 0.01$, $^{***}P < 0.001$. NS, statistically non-significant. See also Figs. S3 and S4.

glycolytic genes (Fig. 5A) and enhanced activity of α-glycerophosphate dehydrogenase (α-GPDH) in their muscle tissues (Fig. 5B), indicating that they had significantly enhanced glycolytic activities. However, we did not detect differences in the levels of lactate in either their serum (Fig. S5A) or skeletal muscle (Fig. S5B). Consistent with these findings, mRNA levels of lactate dehydrogenase (*Ldh*) in muscle was not different between miR-378 Tg and Wt mice (Fig. S5C). Surprisingly, we detected lower levels of pyruvate in the muscle of miR-378 Tg mice than Wt

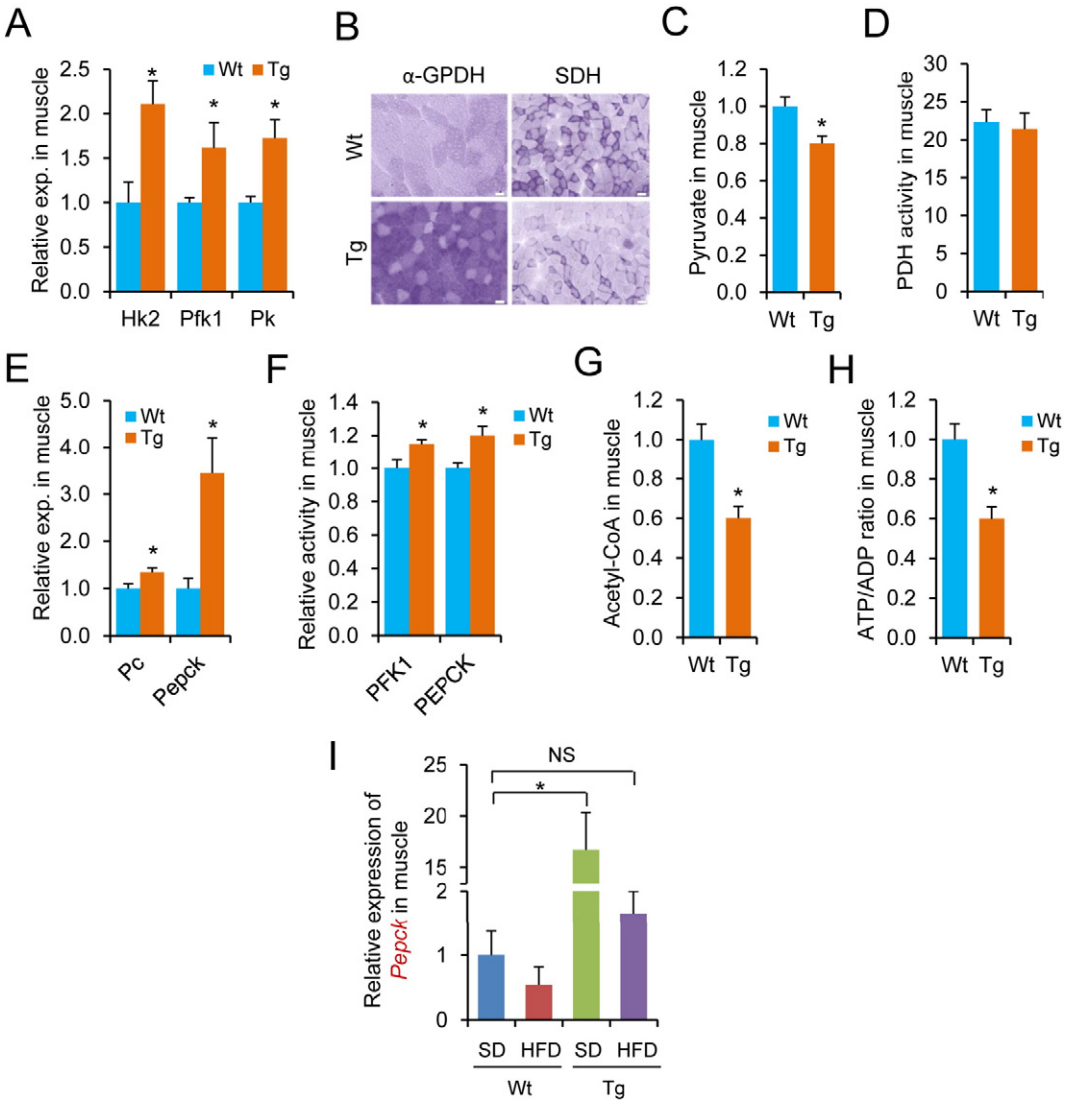

Fig. 5. The pyruvate-PEP futile cycle in skeletal muscle causes energy deficiency in miR-378 Tg mice. (A) Relative expression (exp) of the key glycolytic genes hexokinase 2 (*Hk2*), phosphofructokinase 1 (*Pfk1*), and pyruvate kinase (*Pk*) in skeletal muscle of Wt and Tg mice. (B) Enzymatic staining of α-glycerophosphate dehydrogenase (α-GPDH) and succinate dehydrogenase (SDH), which are enriched in glycolytic and oxidative myofibers, respectively, in *gastrocnemius* muscle of Wt and Tg mice. Images are representative of three mice in each group. Scale bar, 20 μm. (C,D) Pyruvate level (C) and pyruvate dehydrogenase (PDH) activities (D) in *gastrocnemius* muscle homogenates of Wt and Tg mice. (E) Relative expression of the gluconeogenesis genes pyruvate carboxlase (*Pc*) and phosphoenolpyruvate carboxykinase (*Pepck*) in skeletal muscle of Wt and Tg mice. (F) Enzymatic activity of PFK1 and PEPCK in *gastrocnemius* muscle homogenates of Wt and Tg mice. (G) Acetyl-CoA level in *gastrocnemius* muscle homogenates of Wt and Tg mice. (H) ATP/ADP ratio in *gastrocnemius* muscle homogenates of Wt and Tg mice. (I) Relative expression of the *Pepck* gene in *gastrocnemius* muscle of Wt and Tg mice fed an HFD for 8 weeks, respectively. n = 5 male mice in each group. Data are presented as means ± s.e.m. The statistical significance of the difference between two means was calculated using Student's unpaired *t*-test. $^{*}P < 0.05$, $^{**}P < 0.01$. See also Fig. S5.

controls (Fig. 5C), which was not caused by an enhanced activity of pyruvate dehydrogenase (PDH) (Fig. 5D), which converts pyruvate to acetyl-CoA.

Biochemically, a futile cycle occurs when two metabolic pathways run simultaneously in opposite directions, thereby not causing an effect other than to dissipate energy in the form of heat (Schwender et al., 2004). Because increased glycolytic activity did not elevate pyruvate in the muscle tissues of miR-378 Tg mice, we reasoned that pyruvate was converted back to phosphoenolpyruvate (PEP) by a reverse reaction in the pyruvate-PEP futile cycle (Boiteux and Hess, 1981), which is catalyzed by pyruvate carboxlase (PC) and phosphoenolpyruvate carboxykinase (PEPCK). Indeed, we observed significantly increased levels of mRNA (Fig. 5E) and enzymatic activity (Fig. 5F) of PC and PEPCK in the muscle of miR-378 Tg mice compared with Wt controls. We also found that these tissues displayed remarkably decreased levels of acetyl-CoA (Fig. 5G) and ATP (Fig. 5H). Notably, feeding these mice an HFD restored *Pepck* expression to levels similar to that of Wt mice fed a standard diet (SD) (Fig. 5I), indicating that the pyruvate-PEP futile cycle was attenuated when miR-378 Tg mice were provided sufficient energy with an HFD (Fig. 5I). These data implicate that miR-378 activates the pyruvate-PEP futile cycle in skeletal muscle to at least partially cause the energy deficiency seen in miR-378 Tg mice under normal physiological conditions. This implication may explain why miR-378 Tg mice resist HFD-induced obesity (Fig. 3).

3.6. miR-378 Activates the Pyruvate-PEP Futile Cycle via the Akt1-FoxO1-PEPCK Pathway

Next, we investigated the molecular mechanism behind how miR-378 activates the pyruvate-PEP futile cycle in the muscle of miR-378 Tg mice. To identify its target, we first assessed the expression of reported miR-378 targets (Carrer et al., 2012; Eichner et al., 2010; Pan et al., 2014; Ruckerl et al., 2012) (i.e., *Pde1b*, *Pde3b*, *Crat*, *Med13*, *Errγ*, and *Akt1*) (Fig. S6A) and found that only Akt1 expression was significantly

decreased in muscle cells (Figs. S6B and S6C) and tissues of miR-378 Tg mice (Fig. 6A). To learn how miR-378 and Akt1 work together to regulate the pyruvate-PEP futile cycle in these mice, we sought an Akt1-regulated substrate. Interestingly, the transcription factor FoxO1 is a direct substrate of Akt1 (Biggs et al., 1999; Nakae et al., 2001; Rena et al., 1999), and FoxO1 transcriptionally regulates *Pepck*, the key rate-limiting enzyme in the pyruvate-PEP futile cycle (Puigserver et al., 2003). Therefore, we speculated that miR-378 activates the pyruvate-PEP futile cycle by targeting the Akt1-FoxO1-PEPCK pathway. Indeed, we found an increase in the hypophosphorylated (active) form of FoxO1 in the muscle of miR-378 Tg mice. Total FoxO1 protein levels were not overtly different between miR-378 Tg and Wt mice (Fig. 6A).

To confirm that miR-378 activates the pyruvate-PEP futile cycle by targeting the Akt1-FoxO1-PEPCK pathway, we restored the protein levels of Akt1 in miR-378 Tg mice with adenovirus containing a form of Akt without the miR-378-targeting sequence in its 3′-UTR (Ad-CaAkt) (Figs. S6D and S6E). This adenovirus restored protein expression of both total Akt and p-Akt in the muscle of miR-378 Tg mice to levels comparable to Wt mice (Fig. 6B). Moreover, the phosphorylated form of FoxO1 was expressed at similar levels in the muscle of miR-378 Tg and Wt mice (Fig. 6B). Furthermore, restoring Akt1 rescued *Pepck* expression in the muscle of miR-378 Tg mice to the levels comparable to Wt mice (Fig. 6C).

More significantly, in miR-378 Tg mice, restoring Akt1 attenuated lipolysis in WAT (Fig. 6D) and fatty acid use in both BAT (Fig. 6E) and muscle (Fig. 6F). It also restored FFA levels in serum of miR-378 Tg mice (Fig. 6G). Thus, activation of the pyruvate-PEP futile cycle in the muscle is the primary cause for elevated lipolysis in adipose tissues of the miR-378 Tg mice.

3.7. miR-378 Stimulates Lipolysis in WAT by Targeting Scd1

We then examined what miR-378 might target in adipose tissue to promote lipolysis. Interestingly, expression of all the known miR-378 targets, including *Akt1*, remained unchanged in both BAT and WAT of miR-378 Tg mice (Figs. S6F and S6G). We then searched for additional

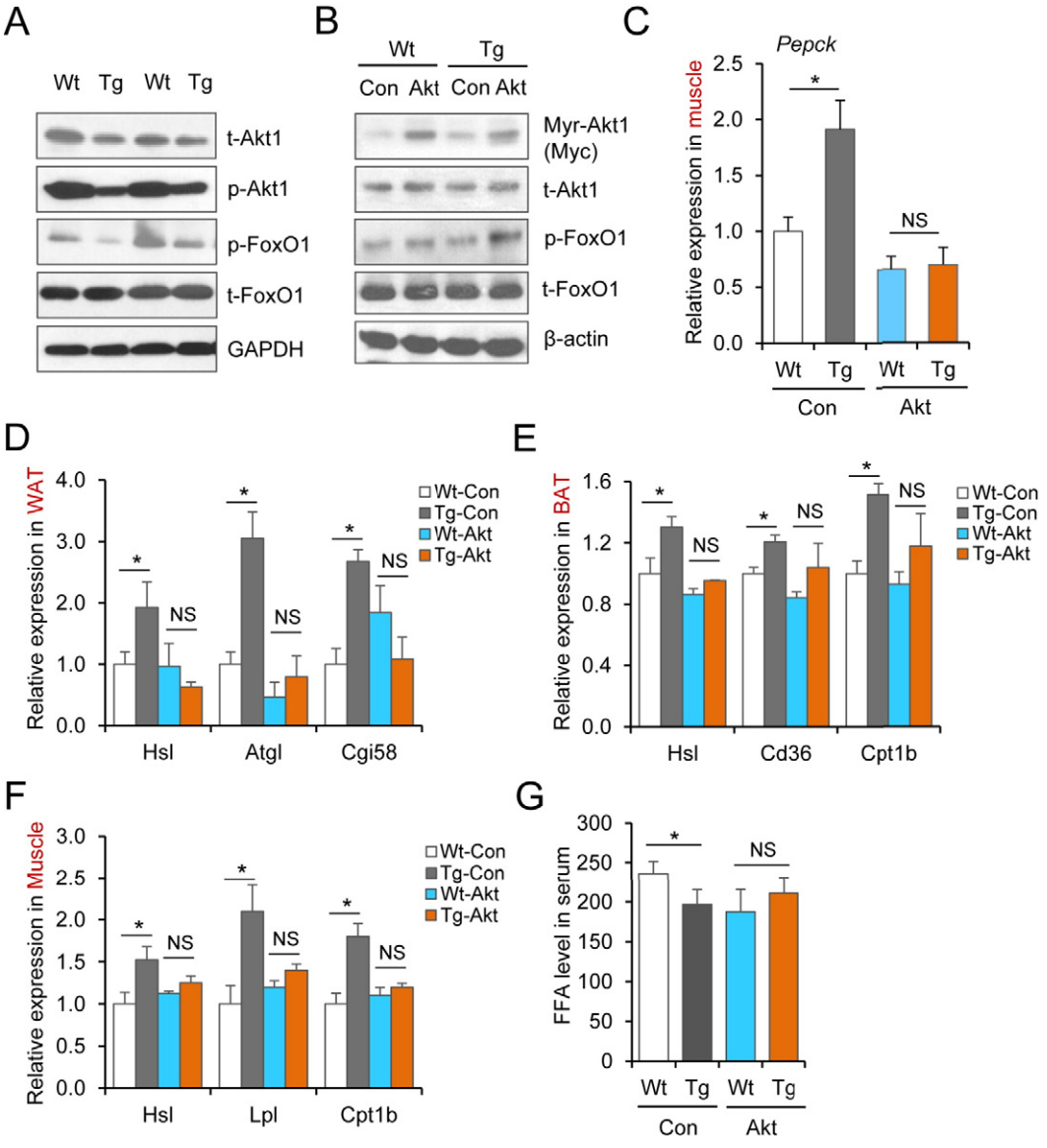

Fig. 6. miR-378 activates pyruvate-PEP futile cycle via the Akt1-FoxO1-PEPCK pathway. (A) Phosphorylated (p-) and total (t-) level of Akt1 and FoxO1 in skeletal muscle of Wt and Tg mice determined by Western blot. GAPDH served as loading control. (B) Adenovirus containing constitutively active Akt1 (Myc-tagged Myr-Akt1) was injected into the tail-vein of Wt and Tg mice. Scramble adenovirus served as control (Con). Ten days after infection, antibodies detected expression of Myc-tagged Myr-Akt1 and phosphorylated (p-) and total (t-) levels of FoxO1 in skeletal muscle by Western blot. β-actin served as loading control. (C) Relative expression of the *Pepck* gene in *gastrocnemius* muscle of Wt and Tg mice described in (B). (D–F) Expression of lipolytic genes in WAT, BAT, and skeletal muscle of mice described in (B). (G) Free-fatty acids (FFA) in serum of mice described in (B). Data are presented as means ± s.e.m. from 5 male mice in each group. The statistical significance of the difference between two means was calculated using Student's unpaired *t*-test. $^*P < 0.05$. NS, statistically non-significant. See also Fig. S6.

miR-378 targets with TargetScan and miRanda. Fortunately, we found that the mRNA of stearoyl-CoA desaturase 1 (*Scd1*) contains a miR-378 binding site in its 3′-UTR (Fig. 7A). *Scd1* catalyzes the production of monounsaturated fatty acids to regulate lipid partitioning between lipogenesis and oxidation (Ntambi, 1995, 1999). Interestingly, *Scd1*-knockout ($Scd1^{-/-}$) mice display a similar phenotype to that of miR-378 Tg mice, including a lean body type and resistance to obesity (Cohen et al., 2002; Miyazaki et al., 2001; Ntambi et al., 2002). We first validated that *Scd1* is a target of miR-378 in HEK-293 cells with luciferase-reporter assays (Fig. 7B). Then we evaluated its expression in adipocytes and found that endogenous *Scd1* was reduced in adipocytes overexpressing miR-378 (Fig. 7C). Interestingly, we also found that overexpressing miR-378 upregulated lipolytic genes in adipocytes (Fig. 7D). Consistent with our *in vitro* data, we observed reduced *Scd1* expression (Fig. 7E) and decreased *Scd1* activity by measuring cellular fatty-acid ratios (C16:1/C16:0 and C18:1/C18:0) in both BAT and WAT of miR-378 Tg mice (Fig. 7F and G). Furthermore, we observed reduced *Scd1* expression in both BAT and WAT of C57BL/6 mice treated with AgomiR-378 and fed an HFD (Fig. 7H). Together, these data support that miR-378 promotes lipolysis in adipose tissues by targeting *Scd1* both *in vitro* and *in vivo*.

4. Discussion

In this report, we not only uncover the pharmacological function of miR-378 in preventing and treating obesity, but we also unravel a unique function of miR-378 in regulating metabolic communication between the muscle and adipose tissues to control energy homeostasis at whole-body levels. miR-378 activates the pyruvate-PEP futile cycle by targeting the Akt1-FoxO1-PEPCK pathway in the muscle, which then enhances lipolysis via miR-378 targeting *Scd1* in adipose tissues. Importantly, we demonstrate that miR-378 activates the pyruvate-PEP futile cycle in skeletal muscle to control whole-body energy homeostasis in mice.

Glycolysis is a metabolic pathway in which glucose is converted to pyruvate to generate two molecules of ATP per molecule of glucose.

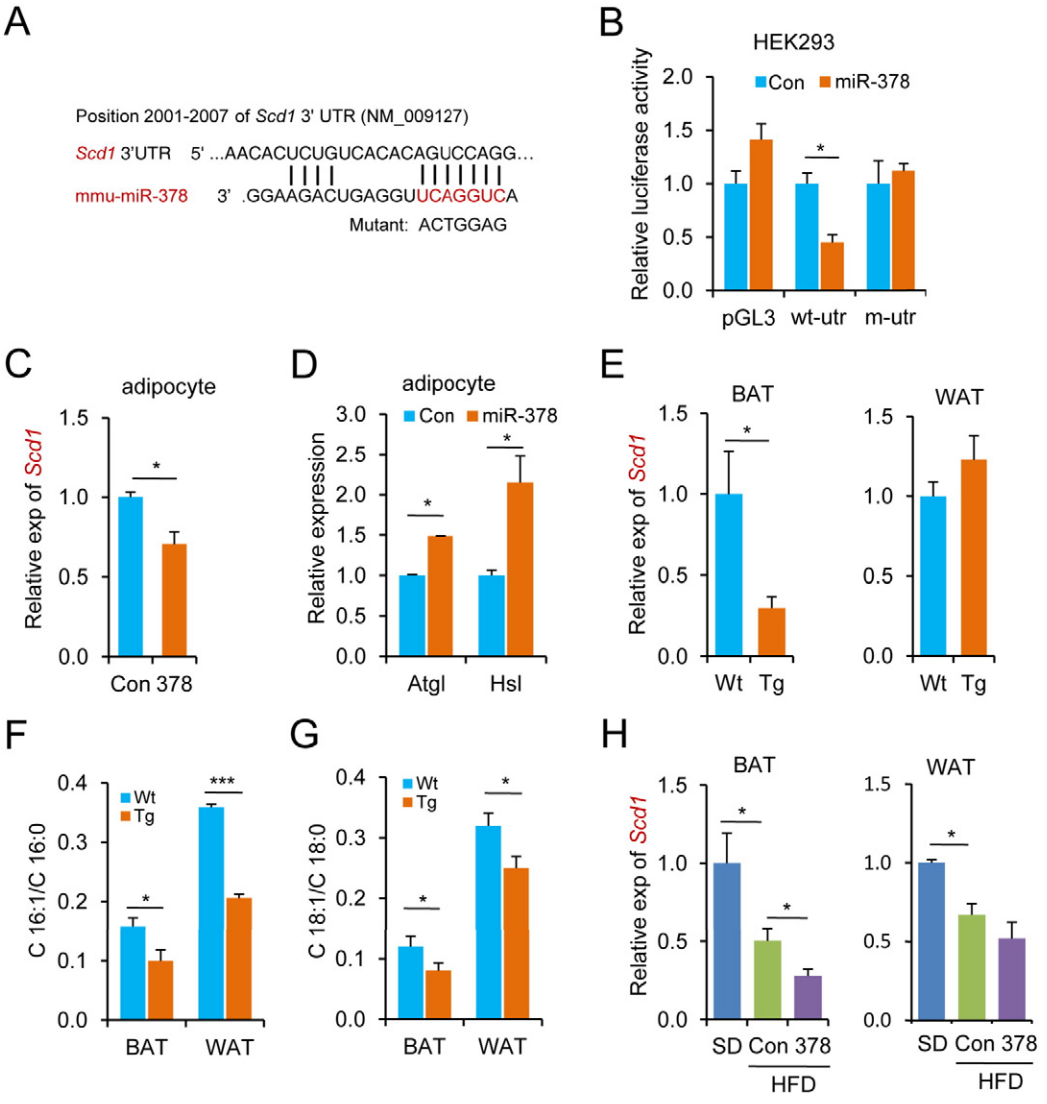

Fig. 7. miR-378 stimulates lipolysis in WAT by targeting *Scd1*. (A) Alignment of miR-378-target sequence in the *Scd1* 3′-UTR predicted with TargetScan. The nucleotide coordinate of *Scd1* was based on the mouse Refseq (NM_009127). Indicated form of UTR (m-utr) was mutated from the seed matches. (B) Effect of miR-378 or a non-specific-control oligonucleotide (NC) on luciferase activity in HEK293 cells expressing the wild-type (wt-utr) or mutated 3′-UTR (m-utr) of *Scd1*. Empty pGL-3 vector served as negative control. Values are means ± s.e.m. of three independent measurements. (C) Expression (exp) of *Scd1* decreased in 3T3-L1-induced adipocytes transfected with miR-378. Values are means ± s.e.m. of three independent experiments. (D) Expression of the lipolytic genes *Hsl* and *Atgl* in 3T3-L1-induced adipocytes described in (C). (E) Reduced expression of *Scd1* in BAT tissues of miR-378 Tg ($n = 5$) and Wt ($n = 5$) mice. (F,G) Decreased SCD1 enzymatic activities in BAT and WAT tissues of Tg mice evidenced by reduced ratios of (F) C16:1/C16:0 and (G) C18:1/C18:0. (H) Reduced expression of *Scd1* in BAT (left) and WAT (right) tissues of AgomiR-378 treated DIO mice ($n = 6$). Data are presented as means ± s.e.m. The statistical significance of the difference between two means was calculated using Student's unpaired *t*-test. $^*P < 0.05$.

Glycolysis is also regulated by futile cycles (Bali and Thomas, 2001), in which two metabolic pathways run simultaneously in opposite directions without an overall effect other than to dissipate energy in the form of heat. In general, futile cycles have been regarded as energetically wasteful reactions that must be avoided in metabolic pathways under normal physiological conditions. However, researchers have speculated that futile cycles may uniquely regulate metabolism to maintain energy homeostasis, especially when energy is rapidly needed (Munakata et al., 2012; Orman et al., 2012; Tolla et al., 2015); although, they have yet to provide data that supports this speculation. In this report, we demonstrated that the miR-378-Akt-FoxO1-PEPCK pathway mediates the pyruvate-PEP futile cycle. Specifically, in miR-378 Tg mice, we found that pyruvate from glycolysis cannot enter the Krebs cycle to produce energy. Instead, it is converted back to PEP in a gluconeogenesis reaction mediated by PEPCK and PC, which costs an ATP molecule and produces an energy deficiency. As a consequence of this futile cycle, more energy from lipolysis is needed to balance energy homeostasis, which is supported by our observation that miR-378 Tg mice have significantly enhanced lipolysis in their adipose tissues. These results suggest that miR-378 activates the pyruvate-PEP futile cycle to orchestrate the glucose–lipid metabolic crosstalk between the muscle and adipose tissues and maintain energy homeostasis. One implication of this finding is that any dysregulated futile cycles of either glucose or fatty acids may be the primary cause of metabolic disorders in humans. Thus, the miR-378-mediated pyruvate-PEP futile cycle or other metabolic futile cycles may serve as promising targets for developing therapies against obesity and/or other metabolic diseases.

We also revealed that *Scd1* is a functional target of miR-378 that promotes lipolysis in adipose tissues of miR-378 Tg mice. SCD1 critically regulates lipid metabolism, and dysregulation of SCD1 activity results in various metabolic disorders, including diabetes, cardiovascular disease, and obesity (Dobrzyn et al., 2015; Sampath and Ntambi, 2011, 2014; Stamatikos and Paton, 2013). Similar to our miR-378 Tg mice, *Scd1*-knockout mice are also resistant to HFD-induced obesity (Cohen et al., 2002; Ntambi et al., 2002). Therefore, in miR-378 Tg mice, we propose a model in which miR-378 activates the Akt1-FoxO1-PEPCK pathway in skeletal muscle to induce the pyruvate-PEP futile cycle, which impairs glucose metabolism and causes energy deficiency. Then, at the same time in adipose tissues, miR-378 directly targets *Scd1* to enhance lipolysis (Fig. S7). Because of miR-378 induced glucose futile cycle, the Tg mice utilize fatty acids to meet energy demand. As a consequence, FFA in the circulation gets low despite of elevated lipolysis in adipose tissues. To validate the primary effect of miR-378-targeted Akt-FoxO1-PEPCK, we used constitutively active Akt1 (ca-Akt1) to rescue the metabolic phenotype of miR-378 Tg mice and observed significantly attenuated lipolysis in ca-Akt1 treated Tg mice. These findings suggest that miR-378 mediates the metabolic communication between muscle and fat by targeting *Akt1* and *Scd1* to regulate systemic energy homeostasis.

It would be very intriguing to identify signals or molecules in mediating the metabolic communications between muscle and fat tissues in miR-378 transgenic mice. Previous publications demonstrate that some metabolites may mediate the regulation of the whole body metabolic homeostasis. For example, insufficient alanine supply mediates a muscle-liver-fat signaling by upregulating FGF21 expression in liver (Shimizu et al., 2015). We observed significantly lower level of pyruvate, lactate, actyl-CoA and FFA in Tg mice than those in wild type control. All of those metabolites are indicators for energy supply, thus the data indicating miR-378 Tg mice suffer severe energy insufficiency. Identifications of the molecules or signals which convey such energy deficiency and mediate inter-organ crosstalk will help us to understand the mechanism of miR-378 in maintaining whole body metabolic homeostasis.

Clinically, our findings support a critical role for miR-378 in human metabolic disorders. Similarly, Kulyté A et al. recently reported that miR-378 was significantly upregulated in cachectic cancer patients, and its expression was strongly and positively associated with catecholamine-stimulated lipolysis in human adipocytes (Kulyte et al., 2014). Their findings suggest that increased miR-378 expression could be an etiological factor in the disease-associated loss of adipose tissue by affecting adipocyte lipolysis and inhibiting disease-induced upregulation of miR-378. Thus, miR-378 may represent a promising target for ameliorating the severity of human diseases caused by impaired lipid metabolism.

Author contributions

Y.Z. and C.L. contributed equally to this work. Y.Z. and C.L. conceived of the study, performed experiments, and drafted the manuscript. H.L. carried out the Western-blot analysis. Y.S. performed fatty acids analysis. Y.Z. conducted tail-vein injections of the Adeno-Akt1 and AgomiR-378 on Tg mice and HFD-fed mice, respectively. L.Z. carried out the luciferase-activity assay of the *Scd1* experiment. H.W. participated in discussion of the experimental design and helped to draft the manuscript. R.Z. served as technical support. H.T. participated in discussion of the experimental design. D.Z. conceived of and supervised the project and wrote the manuscript. The authors declare no competing financial interests.

Acknowledgments

This work was supported by grants from the National Basic Research Program of China (2011CBA01104, 2015CB943103) and the National Natural Science Foundation of China (31271470, 91019010). The funding agencies do not involve in any research activities in the present study.

Appendix A. Supplementary data

Supplementary data to this article can be found online at http://dx.doi.org/10.1016/j.ebiom.2016.01.035.

References

Bali, M., Thomas, S.R., 2001. A modelling study of feedforward activation in human erythrocyte glycolysis. C. R. Acad. Sci. III Sci. Vie 324, 185–199.

Biggs III, W.H., Meisenhelder, J., Hunter, T., Cavenee, W.K., Arden, K.C., 1999. Protein kinase B/Akt-mediated phosphorylation promotes nuclear exclusion of the winged helix transcription factor FKHR1. Proc. Natl. Acad. Sci. U. S. A. 96, 7421–7426.

Bilski, J., Mazur-Bialy, A.I., Brzozowski, B., Magierowski, M., Jasnos, K., Krzysiek-Maczka, G., Urbanczyk, K., Ptak-Belowska, A., Zwolinska-Wcislo, M., Mach, T., et al., 2015. Moderate exercise training attenuates the severity of experimental rodent colitis: the importance of crosstalk between adipose tissue and skeletal muscles. Mediat. Inflamm. 2015, 605071.

Bleau, C., Karelis, A.D., St-Pierre, D.H., Lamontagne, L., 2014. Crosstalk between intestinal microbiota, adipose tissue and skeletal muscle as an early event in systemic low-grade inflammation and the development of obesity and diabetes. Diabetes Metab. Res. Rev.

Boiteux, A., Hess, B., 1981. Design of glycolysis. Philos. Trans. R. Soc. Lond. Ser. B Biol. Sci. 293, 5–22.

Carrer, M., Liu, N., Grueter, C.E., Williams, A.H., Frisard, M.I., Hulver, M.W., Bassel-Duby, R., Olson, E.N., 2012. Control of mitochondrial metabolism and systemic energy homeostasis by microRNAs 378 and 378*. Proc. Natl. Acad. Sci. U. S. A. 109, 15330–15335.

Cohen, P., Miyazaki, M., Socci, N.D., Hagge-Greenberg, A., Liedtke, W., Soukas, A.A., Sharma, R., Hudgins, L.C., Ntambi, J.M., Friedman, J.M., 2002. Role for stearoyl-CoA desaturase-1 in leptin-mediated weight loss. Science 297, 240–243.

Dobrzyn, P., Bednarski, T., Dobrzyn, A., 2015. Metabolic reprogramming of the heart through stearoyl-CoA desaturase. Prog. Lipid Res. 57, 1–12.

Dunn, S.E., Michel, R.N., 1997. Coordinated expression of myosin heavy chain isoforms and metabolic enzymes within overloaded rat muscle fibers. Am. J. Phys. 273, C371–C383.

Eichner, L.J., Perry, M.C., Dufour, C.R., Bertos, N., Park, M., St-Pierre, J., Giguere, V., 2010. miR-378(*) mediates metabolic shift in breast cancer cells via the PGC-1beta/ERR gamma transcriptional pathway. Cell Metab. 12, 352–361.

Hemati, N., Ross, S.E., Erickson, R.L., Groblewski, G.E., MacDougald, O.A., 1997. Signaling pathways through which insulin regulates CCAAT/enhancer binding protein alpha (C/EBPalpha) phosphorylation and gene expression in 3T3-L1 adipocytes. Correlation with GLUT4 gene expression. J. Biol. Chem. 272, 25913–25919.

Kulyte, A., Lorente-Cebrian, S., Gao, H., Mejhert, N., Agustsson, T., Arner, P., Ryden, M., Dahlman, I., 2014. MicroRNA profiling links miR-378 to enhanced adipocyte lipolysis in human cancer cachexia. Am. J. Physiol. Endocrinol. Metab. 306, E267–E274.

Li, P., Oh da, Y., Bandyopadhyay, G., Lagakos, W.S., Talukdar, S., Osborn, O., Johnson, A., Chung, H., Mayoral, R., Maris, M., et al., 2015. LTB4 promotes insulin resistance in obese mice by acting on macrophages, hepatocytes and myocytes. Nat. Med. 21, 239–247.

Liu, W., Cao, H., Ye, C., Chang, C., Lu, M., Jing, Y., Zhang, D., Yao, X., Duan, Z., Xia, H., et al., 2014. Hepatic miR-378 targets p110alpha and controls glucose and lipid homeostasis by modulating hepatic insulin signalling. Nat. Commun. 5, 5684.

Lu, B., Bridges, D., Yang, Y., Fisher, K., Cheng, A., Chang, L., Meng, Z.X., Lin, J.D., Downes, M., Yu, R.T., et al., 2014. Metabolic crosstalk: molecular links between glycogen and lipid metabolism in obesity. Diabetes 63, 2935–2948.

Miyazaki, M., Kim, H.J., Man, W.C., Ntambi, J.M., 2001. Oleoyl-CoA is the major de novo product of stearoyl-CoA desaturase 1 gene isoform and substrate for the biosynthesis of the Harderian gland 1-alkyl-2,3-diacylglycerol. J. Biol. Chem. 276, 39455–39461.

Munakata, K., Ookata, K., Doi, H., Baba, O., Terashima, T., Hirose, S., Kato, A., 2012. Histological demonstration of glucose transporters, fructose-1,6-bisphosphatase, and glycogen in gas gland cells of the swimbladder: is a metabolic futile cycle operating? Biochem. Biophys. Res. Commun. 417, 564–569.

Nakae, J., Kitamura, T., Ogawa, W., Kasuga, M., Accili, D., 2001. Insulin regulation of gene expression through the forkhead transcription factor Foxo1 (Fkhr) requires kinases distinct from Akt. Biochemistry 40, 11768–11776.

Ntambi, J.M., 1995. The regulation of stearoyl-CoA desaturase (SCD). Prog. Lipid Res. 34, 139–150.

Ntambi, J.M., 1999. Regulation of stearoyl-CoA desaturase by polyunsaturated fatty acids and cholesterol. J. Lipid Res. 40, 1549–1558.

Ntambi, J.M., Miyazaki, M., Stoehr, J.P., Lan, H., Kendziorski, C.M., Yandell, B.S., Song, Y., Cohen, P., Friedman, J.M., Attie, A.D., 2002. Loss of stearoyl-CoA desaturase-1 function protects mice against adiposity. Proc. Natl. Acad. Sci. U. S. A. 99, 11482–11486.

Olshansky, S.J., Passaro, D.J., Hershow, R.C., Layden, J., Carnes, B.A., Brody, J., Hayflick, L., Butler, R.N., Allison, D.B., Ludwig, D.S., 2005. A potential decline in life expectancy in the United States in the 21st century. N. Engl. J. Med. 352, 1138–1145.

Orman, M.A., Androulakis, I.P., Berthiaume, F., Ierapetritou, M.G., 2012. Metabolic network analysis of perfused livers under fed and fasted states: incorporating thermodynamic and futile-cycle-associated regulatory constraints. J. Theor. Biol. 293, 101–110.

Pan, D., Mao, C., Quattrochi, B., Friedline, R.H., Zhu, L.J., Jung, D.Y., Kim, J.K., Lewis, B., Wang, Y.X., 2014. MicroRNA-378 controls classical brown fat expansion to counteract obesity. Nat. Commun. 5, 4725.

Puigserver, P., Rhee, J., Donovan, J., Walkey, C.J., Yoon, J.C., Oriente, F., Kitamura, Y., Altomonte, J., Dong, H., Accili, D., et al., 2003. Insulin-regulated hepatic gluconeogenesis through FOXO1-PGC-1alpha interaction. Nature 423, 550–555.

Rena, G., Guo, S., Cichy, S.C., Unterman, T.G., Cohen, P., 1999. Phosphorylation of the transcription factor forkhead family member FKHR by protein kinase B. J. Biol. Chem. 274, 17179–17183.

Ruckerl, D., Jenkins, S.J., Laqtom, N.N., Gallagher, I.J., Sutherland, T.E., Duncan, S., Buck, A.H., Allen, J.E., 2012. Induction of IL-4Ralpha-dependent microRNAs identifies PI3K/Akt signaling as essential for IL-4-driven murine macrophage proliferation in vivo. Blood 120, 2307–2316.

Sampath, H., Ntambi, J.M., 2011. The role of stearoyl-CoA desaturase in obesity, insulin resistance, and inflammation. Ann. N. Y. Acad. Sci. 1243, 47–53.

Sampath, H., Ntambi, J.M., 2014. Role of stearoyl-CoA desaturase-1 in skin integrity and whole body energy balance. J. Biol. Chem. 289, 2482–2488.

Schwender, J., Ohlrogge, J., Shachar-Hill, Y., 2004. Understanding flux in plant metabolic networks. Curr. Opin. Plant Biol. 7, 309–317.

Shimizu, N., Maruyama, T., Yoshikawa, N., Matsumiya, R., Ma, Y., Ito, N., Tasaka, Y., Kuribara-Souta, A., Miyata, K., Oike, Y., et al., 2015. A muscle-liver-fat signalling axis is essential for central control of adaptive adipose remodelling. Nat. Commun. 6, 6693.

Stamatikos, A.D., Paton, C.M., 2013. Role of stearoyl-CoA desaturase-1 in skeletal muscle function and metabolism. Am. J. Physiol. Endocrinol. Metab. 305, E767–E775.

Tolla, D.A., Kiley, P.J., Lomnitz, J.G., Savageau, M.A., 2015. Design principles of a conditional futile cycle exploited for regulation. Mol. BioSyst. 11, 1841–1849.

Viscarra, J.A., Ortiz, R.M., 2013. Cellular mechanisms regulating fuel metabolism in mammals: role of adipose tissue and lipids during prolonged food deprivation. Metab. Clin. Exp. 62, 889–897.

Wu, R., Li, H., Li, T., Zhang, Y., Zhu, D., 2015a. Myostatin regulates miR-431 expression via the Ras-Mek-Erk signaling pathway. Biochem. Biophys. Res. Commun. 461, 224–229.

Wu, R., Li, H., Zhai, L., Zou, X., Meng, J., Zhong, R., Li, C., Wang, H., Zhang, Y., Zhu, D., 2015b. MicroRNA-431 accelerates muscle regeneration and ameliorates muscular dystrophy by targeting Pax7 in mice. Nat. Commun. 6, 7713.

Xu, Z., Harvey, K., Pavlina, T., Dutot, G., Zaloga, G., Siddiqui, R., 2010. An improved method for determining medium- and long-chain FAMEs using gas chromatography. Lipids 45, 199–208.